Pyrene-based cationic fluorophores with high-affinity for BF_4^-, PF_6^- and ClO_4^- Anions: detection and removal

Xu Zhou,[a,b] Xiaohui Wang,[c] Tian-Yu Zhang,[a,b] Lingyi Shen,[a,b] Xian-Jiong Yang,[a,b] Qi-Long Zhang,*[a,b] Hong Xu,*[a,b] Carl Redshaw[d] and Xing Feng*[c]

[a] School of Biology and Engineering, Guizhou Medical University, Guiyang 550025, PR China.

[b] School of Basic Medicine, Guizhou Medical University, Guiyang 550025, PR China.

[c] Guangdong Provincial Key Laboratory of Functional Soft Condensed Matter, School of Material and Energy, Guangdong University of Technology, Guangzhou 510006, PR China.

[d] Chemistry, School of Natural Sciences, University of Hull, Cottingham Road, Hull, Yorkshire HU6 7RX, UK.

Abstract: Anions play an indispensable role in the balance and regulation of the ecological environment and human health, however, excess anions can cause serious ecological and environment problems. Therefore, the detection and removal of excess anions in aqueous solution is not only a technological problem, but also crucial for environmental protection. Herein, a set of water-soluble pyrene-based cationic fluorophores were synthesized, which exhibit high sensitivity for the detection of the anions BF_4^-, PF_6^- and ClO_4^- via electrostatic interactions. Such fluorescent probes exhibit "turn-on" emission characteristics even at low concentration of anions due to anion-π^+ interactions. Moreover, these fluorescence probe act as efficient precipitating agents for the removal of the BF_4^-, PF_6^- and ClO_4^- anions from an aqueous environment. This example opens up new avenues for future research on pyrene-based fluorophores as turn-on fluorescence probes for anion detection and as excellent precipitating agents in environmental settings.

1. Introduction

Molecular self-assembly is spontaneous behaviour via weak intra-/intermolecular interactions (such as electrostatic interactions, van der Waals' forces, H-bonding etc.).[1] Among them, the electrostatic interaction occurs between cations and anions with a relatively strong interaction without direction, and is one of the important driving forces for the formation of supramolecular architectures,[2] molecular recognition[3] and in protein folding.[4]

Anions illustrating a 3D spatial structure, such as BF_4^- and PF_6^- , have been widely used as ionic liquids in catalysis and in the lithium-ion battery industry.[5,6] However, their extensive application has also caused a series of environmental issues. For example, as lithium-ion technology has developed, new energy vehicles have entered our everyday life, but this has also led to new challenges such as how to recycle the lithium-ion batteries as well as electrolytes.[7] On the other hand, perchlorate (ClO_4^-) is a new type of persistent inorganic pollutant, which can exhibit fast diffusion, high stability and is problematic to the environment. Moreover, even at low concentrations, ClO_4^- can also cause serious ecological issues and be detrimental to human health.[8] Thus, much effort is focussed on exploring high-tech ways for the specific detection and recycling of this category of anion. Traditional methods are based on electrochemistry,[9.10] ion chromatography,[11,12] atomic absorption spectroscopy, and spectrophotometry,[13,14] but these technologies still exhibit a number of disadvantages, such as poor reproducibility, long duration, low sensitivity, etc.

Thus, it is of vital practical significance to develop new methods for identifying BF_4^-, PF_6^- and ClO_4^- anions, as well as ways of removing them.

Fluorescent probes[15-19] have emerged as powerful tools in recent years and have been exploited for determining metal ions and anions in various environments. Compared with the above-mentioned methods, fluorescent technologies possess some unique advantages such as simplicity, high speed, high sensitivity, high resolution and high selectivity.[20-22] However, compared to the fast-growing field of fluorescent probes for cation detection, it remains a challenge to design highly specific and sensitive fluorescence probes for anion detection.[23-24] The main reason is that anions have multiple geometries with larger ionic radius, which make them more sensitive to pH and imparts higher hydration energy.[25] On the other hand, solvents can preferentially and specifically bind the probe molecule rather than the anion, and the higher polarity of the solvent could aggravate this competitive relationship, resulting in poor anion detection. Therefore, the development of ideal fluorescent probes for anion detection is rare.

In 2001, Tang with co-workers observed a new type lumingenous, namely silole, which was non-emissive in solution, but with enhanced emission in the aggregation state.[26] This phenomenon was defined as aggregation-induced emission (AIE). High-efficiency organic materials with AIE characteristics have been widely used in environmental analysis and for bio-sensing in view of their abnormal optical properties.[27-30] Inspired by electrostatic interactions, cationic

fluorescence probes with AIE characteristic have been explored for detecting various anions. Flood *et al*.[31] reported a macrocycle that can specifically binding with BF_4^-, PF_6^- and ClO_4^- in a MeOH/CH_2Cl_2 system with a large binding constant, due to the synergetic effect of electrostatic interactions and a number of hydrogen-bonding interactions between the host-guest molecules. Kumar and Singh *et al*. used a biphenyl linked bisbenzimidazolium fluorescent probe to achieve the highly selective recognition of ClO_4^-.[32,33] Moreover, our group has also developed a series of cationic water-soluble AIE fluorescent probes for anion detection via electrostatic interactions and weak interactions, such as Van der Waals forces and π-π interactions.[34-38] On the other hand, due to the presence of strong electrostatic interactions, the probe also can rapidly capture various anions which readily affiliate to form neutral clusters, thereby resulting in insoluble species, which can be removed by facile processes, and this could open up a potential pathway for the exploitation of ionic fluorescent probes as a tool for bringing the ionic contaminants (such as metal ions and anions) under control.

Pyrene possesses a strong monomer or excimer emission in solution, depending on the degree of aggregation, and can be utilized as a fluorescence probe for metal ion detection.[39-42] Moreover, pyrene displays a sensitivity to the polarity of the solvent.[43] Herein, a set of water-soluble, turn-on type pyrene-based acceptor-π-acceptor (A-π-A) cationic fluorescent probes **DPPD-R** [4,4'-((1E,1'E)-pyrene-1,6-diylbis(ethene-2,1-diyl))bis(1-nonylpyridin-1-ium) (**DPPD-9C**), 4,4'-((1E,1'E)-pyrene-1,6-diylbis(ethene-2,1-diyl))bis(1-

nonylpyridin-1-ium) (**DPPD-10C**) and 4,4'-((1E,1'E)-pyrene-1,6-diylbis(ethene-2,1-diyl))bis(1-dodecylpyridin-1-ium) (**DPPD-12C**)] and the intermediate 1,6-bis((E)-2-(pyridin-4-yl)vinyl)pyrene (**DPPD**) were synthesized. Here, the pyrene not only acts as a π-bridge, but also can be a donating group for constructing a pull-push electronic structure. Moreover, the pyridine unit with a positive charge can be a recognition group for identifying and trapping anions. Indeed, the cationic pyrene-based probes not only show a highly affinity for detecting BF_4^-, PF_6^- and ClO_4^- anions via electrostatic interactions, but also can remove them in near quantitative fashion from an aqueous environment.

RESULTS AND DISCUSSION

*3.1 Design and synthesis of **DPPD** and **DPPD-R***

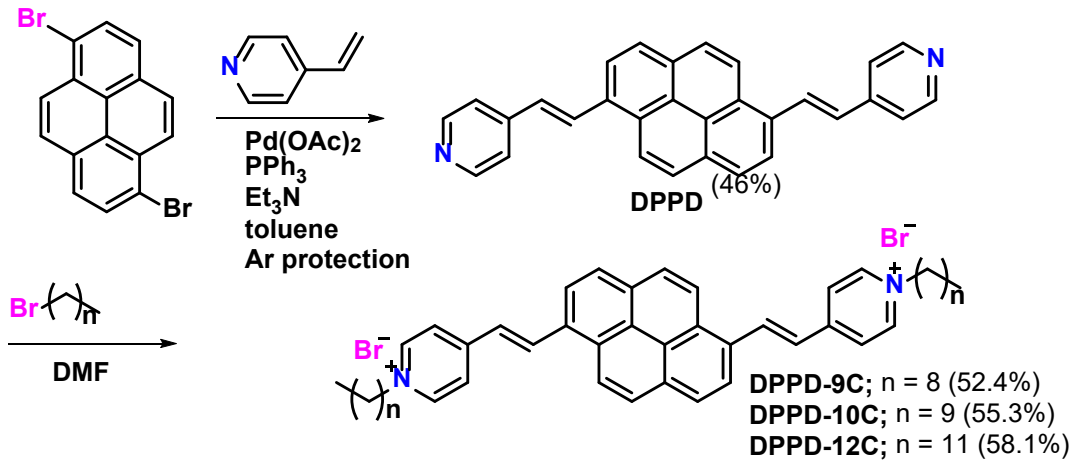

Scheme 1. *Design and synthesis of **DPPD** and **DPPD-R***

The synthetic **routes for DPPD** and **DPPD-R** are shown in (Scheme 1). The structure of **DPPD** was characterized by single crystal X-ray diffraction analysis, NMR spectroscopy and HRMS (Figs. S1- S9).

3.2. Single crystal X-ray diffraction analysis of ***DPPD***

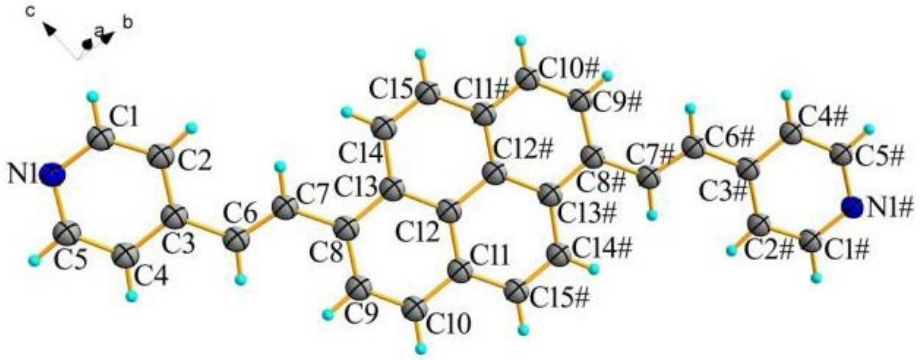

Fig. 1. X-ray structure of **DPPD**. (Symmetry code: #-x, -y, -z. ORTEP representation of the symmetry expanded local structure for **DPPD** showing 30% thermal ellipsoids.)

Compound **DPPD** was dissolved in a mixed solvent system of trichloromethane and ethyl acetate. Single crystals of **DPPD** suitable for single crystal X-ray diffraction were grown by slow evaporation of the solvent, and the X-ray structure of DPPD is presented in Fig.1; key crystal structural refinement parameters are summarized in Table S1. The crystal belongs to the orthorhombic system with the space group Pbca, and the asymmetric unit contains one molecule of **DPPD** with two $CHCl_3$ solvent molecules. As shown in Fig.1, the pyrene connects to two pyridine ring molecules through double bonds. The two double bonds are in a "*trans*-configuration". The two pyridine rings are almost coplanar with the pyrene core, and the dihedral angle between the pyrene and the pyridine ring is 169.26º. In the packing, the structure prefers to arrange with herringbone-type packing with a J-aggregation model by several groups of C-H···π interactions at a distance of 3.5~3.7 Å (Table S2).

3.3. Photophysical properties of ***DPPD-R***

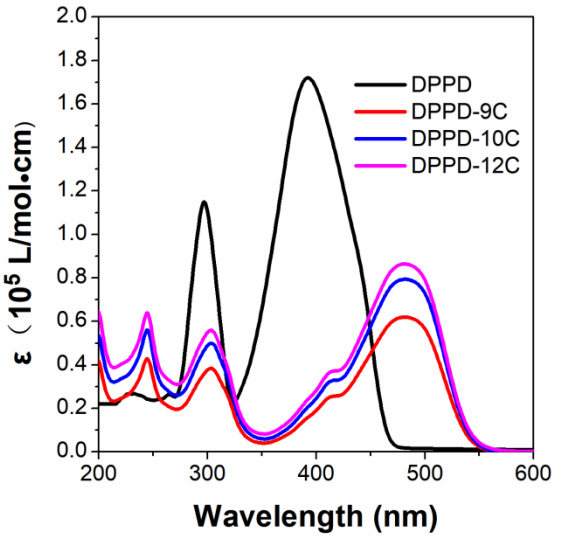

Fig. 2. UV-vis spectra of three compounds (each of 10.0 μM) in MeOH at 25 °C.

The UV-vis absorption spectra of **DPPD** and **DPPD-R** were investigated in MeOH solution (10^{-5} M). As shown in Fig.2, **DPPD** exhibits a maximum absorption peak at 400 nm, with a molar absorption coefficient of 1.783×10^{3} m^{-1} cm^{-1}. The **DPPD-9C**、**DPPD-10C** and **DPPD-12C** exhibit a similar absorption band in the range of 200-550 nm, indicating that the length of the terminal alkyl chain has a limited effect on the absorption peak and the maximum absorption bands are at 482 nm. However, as the length of the alkyl chain increases, the mole extinction coefficient increases in the following order **DPPD-12C** (8.640×10^{4} m^{-1} cm^{-1}) > **DPPD-10C** (7.937×10^{4} m^{-1} cm^{-1}) > **DPPD-9C** (6.194×10^{4} m^{-1} cm^{-1}).

On the other hand, the compounds **DPPD-R** show good solubility in polar solvents, such as H_2O, methanol, but are insoluble in $CHCl_3$. Thus, the emission spectra of the three compounds were measured in MeOH and a mixture of MeOH/$CHCl_3$ with

different $CHCl_3$ fractions (f_{CHCl3}) and are presented in Figs. 3 and S10. Compared to the cyan blue emission of **DPPD** (480 nm), the **DPPD-9C**、**DPPD-10C** and **DPPD-12C** exhibit a weak red emission with a maximum emission peak at 597 nm for **DPPD-9C**, 598 nm for **DPPD-10C** and 598 nm for **DPPD-12C**, respectively, which is attributed to the strong acceptor-donor-acceptor structure, where the cationic pyridine ring acts as a strong electron-withdrawing group, and the pyrene as an electron-donating group.[35] Moreover, the alkyl chains at pyridine exert a limited effect on the emission behavior. Taking **DPPD-10C** as an example, the fluorescence intensity gradually increased as the $CHCl_3$ content increased, and when the f_{CHCl3} reached 60%, the compound **DPPD-10C** shows a maximum emission peak at 610 nm. Subsequently, the fluorescence intensity has slightly decreased when the $CHCl_3$ content reached 90%. Although the compounds exhibit an enhanced emission in the mixture MeOH/$CHCl_3$, the compounds present a low quantum yield in the solid state compared to in solution (Table 1). We speculate that the expanding π-conjugated molecules with large planar structures can form a strong *J*-aggregation in the solid state, resulting in quenched fluorescence.[44]

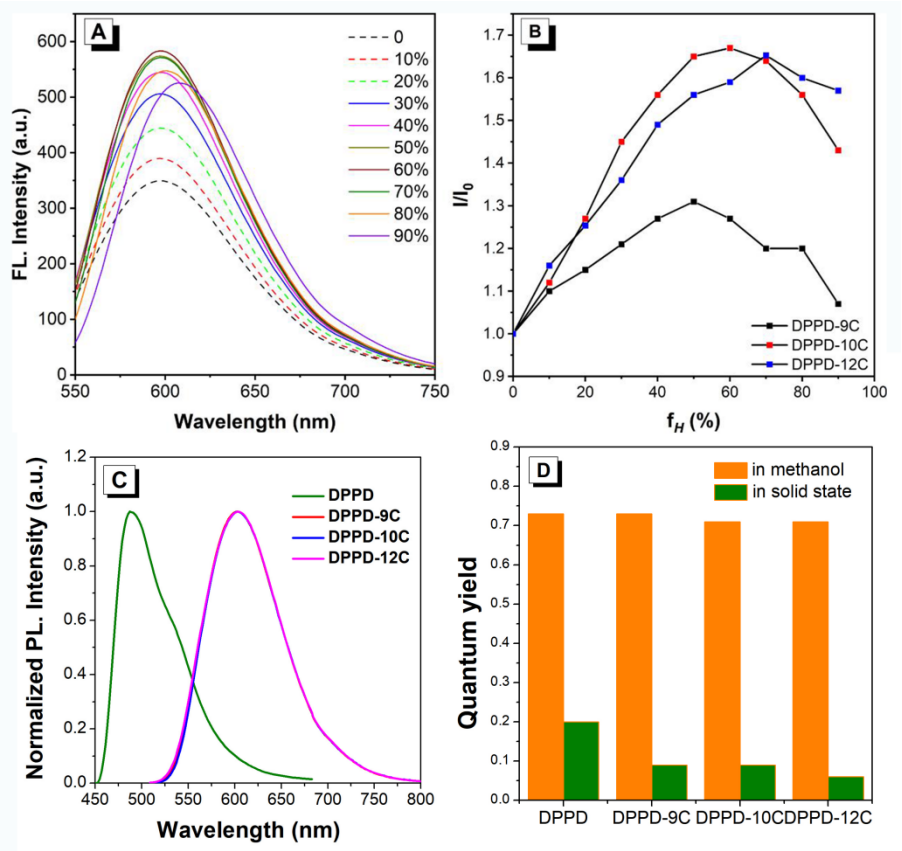

Fig. 3. Fluorescence spectra of **DPPD-10C** (A) **DPPD-10C** and (B) Plots of AIE curves in MeOH/$CHCl_3$ with different $CHCl_3$ fraction (f_{CHCl3}) (λex = 485nm). (C) the emission spectra of the compounds. (D) Fluorescence quantum yield of **DPPD** and **DPPD-R** in solution and in solid state.

Table 1. Absorption, emission and fluorescence quantum yield data of pyrene compounds **DPPD-9C**, **DPPD-10C** and **DPPD-12C**.

Compound	$\lambda_{max\ abs}$ [nm][a]	λ_{maxPL}[nm]	Φ_f
	$\varepsilon\times10^4$[$M^{-1}cm^{-1}$]	Solns[a]/films[b]	Solns[a]/films[b]
DPPD	412 (3.07)	485	0.72 / 0.20
DPPD-9C	481 (6.20)	597	0.73 / 0.09

DPPD-10C	481 (7.94)	598	0.71 / 0.09
DPPD-12C	481 (8.64)	598	0.71 / 0.06

a) Maximum absorption wavelength; b) Measured in MeOH solution at room temperature; c) Measured in the solid state.

3.4. Anion recognition properties of ***DPPD-R***

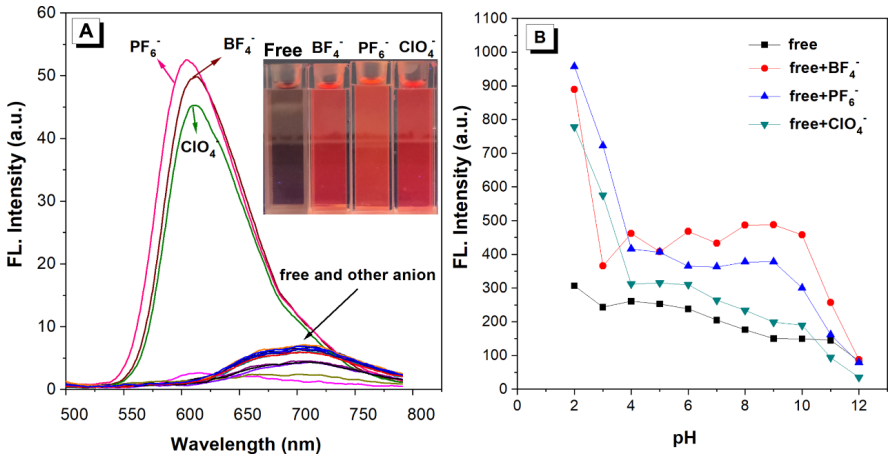

Fig. 4. (A) Fluorescence spectra of **DPPD-10C** (10.0 μM) in water in the presence of various anions including F^-, Cl^-, Br^-, I^-, SO_3^{2-}, SO_4^{2-}, BF_4^-, PF_6^-, ClO_4^-, PO_4^{3-}, HPO_4^{2-}, NO_2^-, NO_3^-, HCO_3^-, CO_3^{2-} and CH_3COO^- (each of 20 equiv.). (λex = 485 nm). (B) Changes of fluorescence intensity of **DPPD-10C** (10.0 μM) before and after response with target anion (each of 20 equiv.) in aqueous solutions with different pH values (λex = 480 nm).

Further, the three pyrene-based cationic fluorophores **DPPD-9C**, **DPPD-10C** and **DPPD-12C** were selected as fluorescence probes for metal detection, which comprised a mixture with 20 times of the concentration of various anions (such as F^-, Cl^-, Br^-, I^-,

SO_3^{2-}, SO_4^{2-}, BF_4^-, PF_6^-, ClO_4^-, PO_4^{3-}, HPO_4^{2-}, NO_2^-, NO_3^-, HCO_3^-, CO_3^{2-} and CH_3COO^-) in a mixture of MeOH/H_2O with f_w = 90% at pH = 7.0, respectively. As shown in Figs. 4A and S11, as the anions were added, the maximum emission peak of each compound was red-shifted to 700 nm with decreased emission intensity. Meanwhile in the presence of the anions BF_4^-, PF_6^- or ClO_4^-, the emission intensity was enhanced *ca* 10-fold with a maximum emission peak at 610 nm. Clearly, all the red emitters show a high-affinity to the anions BF_4^-, PF_6^- and ClO_4^-. We infer that the dominant driving force is the electrostatic interactions between the target anions and the positively charged probes,[32-38] which induce the formation of anion - π^+ interactions, resulting in enhanced emission via molecular aggregates.[45] Dynamic light scattering experiment shows that after **DPPD-R** interacts with the target anion, its average particle size increases (Table 2, Figure S12-S14). This result further confirms our conjecture.

Table 2. Dynamic light scattering data.

Compound	Average particle size (nm)			
	Blank	BF_4^-	PF_6^-	ClO_4^-
DPPD-9C	5.8	289.9	310.8	301.3
DPPD-10C	11.1	296.2	312.6	305.8
DPPD-12C	25.6	310.8	328.1	312.5

Furthermore, to investigate the effect of pH on the anion detection, the fluorescence spectra were recorded in the range of pH = 4 ~ 10. It was found that the pH value exerts only a slight effect on the detection of the three anions BF_4^-, PF_6^- and

ClO_4^- (Figs. 4B and S15). Thus, the probes can effectively detect the target anions over the range of pH = 4~10. Furthermore, interference experiments were measured for investigating the effect of coexisting anions (such as F^-, Cl^-, Br^-, I^-, SO_3^{2-}, SO_4^{2-}, BF_4^-, PF_6^-, ClO_4^-, PO_4^{3-}, HPO_4^{2-}, NO_2^-, NO_3^-, HCO_3^-, CO_3^{2-} and CH_3COO^-) on the detection of the three anions BF_4^-, PF_6^- and ClO_4^-. The experimental results indicated that the coexist anions exerted only a slight interference on this system. (Figure S16).

Under the optimized experimental conditions, interference tests were performed to investigate the effect of other anions on the recognition of BF_4^-, PF_6^- and ClO_4^- by the pyrene-based emitters (Figure S17). The emission spectra of the three fluorescence probes reveal no obvious changes in the presence or absence of interfering anions in the solvent contains BF_4^-, PF_6^- and ClO_4^- anions, indicating that the coexisting anions did not affect the fluorescence probe to identify the target anion. In addition, fluorescence titration experiments were further carried out to determine the limit of detection of the three fluorescence probes for BF_4^-, PF_6^- and ClO_4^- anions (Figures S18-S20). It was found that the detection limits of the probes for the target anions gradually decreased from 1.063 to 3.786 μM for BF_4^-, 0.622 to 1.969 μM for PF_6^- and 1.162 to 2.283 μM for ClO_4^- on increasing the alkyl chain length of the probes (Table 3). Thus, the three pyrene-based AIEgens are excellent fluorescence probes for detecting the BF_4^-, PF_6^- and ClO_4^- anions with high selectivity and with a low limit of detection in various environments.

Table3. **DPPD-R** probe was used as a fluorescent reagent for the analytical parameters of anions.

Probe	anions	linear range of correction curve M	R^2	LOD μM
DPPD-9C	BF_4^-	5.0×10^{-6}~3.0×10^{-5}	0.998	3.786
	PF_6^-	1.0×10^{-6}~1.4×10^{-5}	0.999	1.969
	ClO_4^-	1.0×10^{-6}~1.4×10^{-5}	0.995	2.283
DPPD-10C	BF_4^-	1.5×10^{-5}~4.0×10^{-5}	0.993	2.620
	PF_6^-	1.0×10^{-6}~1.2×10^{-5}	0.996	0.626
	ClO_4^-	3.0×10^{-6}~1.5×10^{-5}	0.990	1.779
DPPD-12C	BF_4^-	1.0×10^{-5}~8.0×10^{-5}	0.998	1.063
	PF_6^-	2.0×10^{-6}~1.6×10^{-5}	0.997	0.622
	ClO_4^-	2.0×10^{-6}~1.1×10^{-5}	0.996	1.162

*3.5. Anion adsorption properties of **DPPD-R***

More interestingly, when mixing each pyrene-based fluorescence probe with BF_4^-, PF_6^- or ClO_4^- anions (mole ratio: 1:20) in the MeOH/H_2O=1:9 solvent mixture for 1 h, respectively, an amount of red suspended solid was observed. Also, the precipitates were filtered and analyzed by scanning electron microscopy (SEM). Taking **DPPD-10C** as an example, as shown in Fig.5, the **DPPD-10C** had self-assembled into a plate-like morphology in the aggregate state, when the fluorescence probe met the target anions of BF_4^-, PF_6^- or ClO_4^-; the morphology was changed to a uniform ball-like, irregular fiber-like and gel-like assemblies, respectively. The formation of these morphologies may be due to the different anion molecular geometries and the ionic radii (Figure 5d.). For example, a regular tetrahedral configuration for BF_4^-, an octahedral configuration for PF_6^- and the different ionic radii of BF_4^- and ClO_4^-, thus affecting the self-assembly mechanism of the probes. Additionally, X-ray electron spectroscopy (EDS) elemental analysis showed that trace B, P and Cl elements were uniformly distributed in the nanoparticles. These results indicated that the target anions

prefer to associate around the fluorescence probe via electrostatic interactions. Furthermore, the suspended solids became clearer as the concentration of added BF_4^-, PF_6^- and ClO_4^- anions increased from 0 to 20 mM in the pyrene-based fluorescence probe (100 μM), respectively, indicated that the fluorescence probes also act a precipitating agent to remove BF_4^-, PF_6^- and ClO_4^- anions from the aqueous environment. This is of potential application in terms of environmental pollution control.

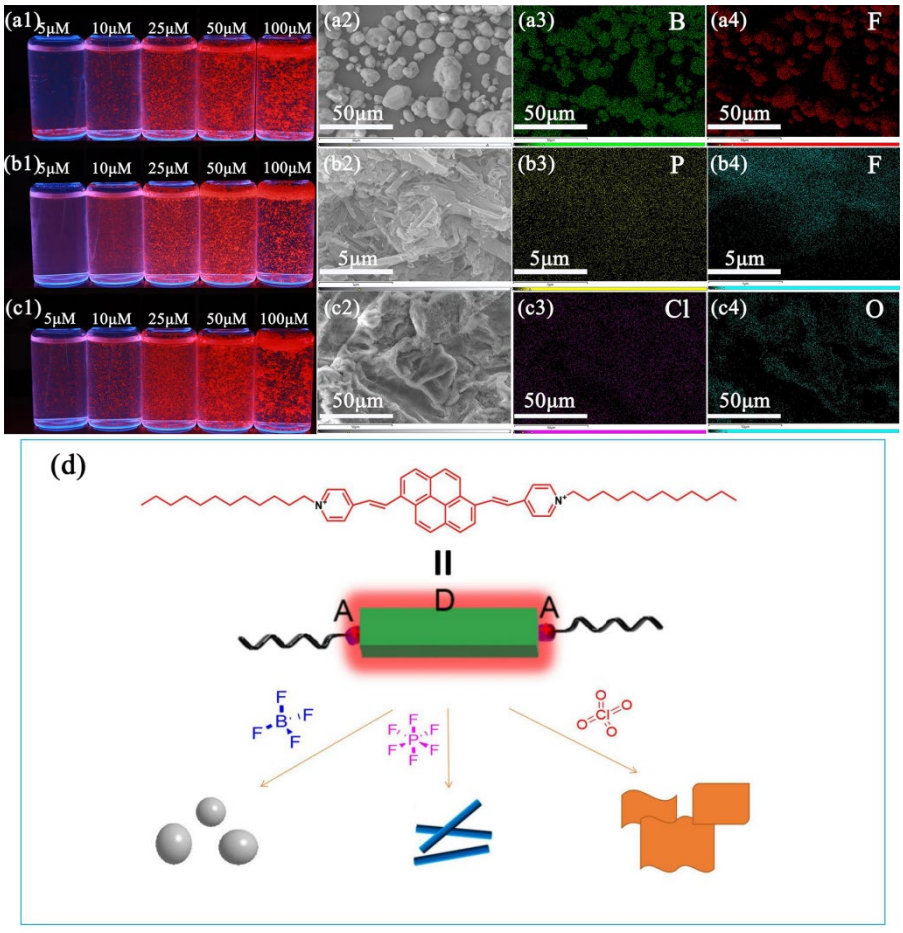

Fig. 5. Photographs of **DPPD-10C** in the presence of (a1) BF_4^-, (b1) PF_6^- and (c1) ClO_4^- ions after 6 h under UV light (360 nm). SEM image of (a2) BF_4^-, (b2) PF_6^- and (c2) ClO_4^- induced precipitates of **DPPD-10C**. EDS image of (a3-

a4) BF_4^-, (b3-b4) PF_6^- and (c3-c4) ClO_4^- induced precipitates of **DPPD-10C**. (d) Proposed mechanism for anions recognition triggered self-assembly of probes in aqueous media.

CONCLUSIONS

In summary, we have designed and synthesized three water-soluble cationic pyrene-based probes containing a pyridine unit, which exhibit light-up fluorescence with a high-affinity towards BF_4^-, PF_6^- and ClO_4^- anions via electrostatic interactions in an aqueous environment. The fluorescence probes possess a relative low detection limit for the BF_4^-, PF_6^- and ClO_4^- anions at 1.063 μM, 0.622 μM and 1.162 μM, respectively. Moreover, these fluorescence probes can interact with these anions to form precipitates by self-assembly in aqueous solution. Thus, these compounds are not only excellent light-up fluorescence probes for detecting anions, but also can be employed as a precipitating agent for the removal of high concentrations of anions, which provides a new tool for the management of anionic pollutants in environment and industrial arenas.

EXPERIMENTAL SECTION

Materials and instrumentation. All chemical materials used in this st udy were obtained from commercial suppliers and were not further purifi ed. Silica gel (Guiyang Chaoyuan Zhi-Cheng Biotechnology Co.) was use d for column chromatography. ^1H NMR were measured on a Bruker Ava nce III, and chemical shifts are reported in ppm (in $CDCl_3$ and d6-DMS O, TMS is the internal standard). Absorption spectra were recorded on a

UV-2600 spectrophotometer. Fluorescence emission spectroscopy was perfo rmed on a Cary eclipse fluorescence spectrometer from Varian, USA. Sca nning Electron Microscopy (SEM) was carried out using a Hitachi S-480 0 II field-emission SEM system. Samples were deposited on a SiO_2/Si su bstrate and dried in air at room temperature. ESI-TOF mass spectra were obtained with an Agilent HPLC-6545.

Synthesis of 1,6-di(4-vinylpridine) pyrene (**DPPD**) and **DPPD-R**. **DPPD: A** mixture of 1,6-dibromopyrene (0.72 g, 2 mmol), 4-vinylpridine (1.06 g, 10mmol), Pd $(OAc)_2$ (50 mg, 0.223 mmol), triphenylphosphine (0.525 g, 2 mmol) were added into a mixture solvent of triethylamine (5 mL) and toluene (5 mL), and the system was stirred at 105℃ (an oil bath) for 72h under an argon atmosphere. After the reaction was complete, the mixture was cooled to room temperature and quenched by water (20 mL), extracted by dichloromethane and washed twice by water (50 mL x2), and brine, and then the combined organic layer was dried by anhydrous magnesium sulfate and evaporated. The residue was recrystallized from toluene to obtain a yellow solid (**DPPD**). (0.38 g, 46%). mp 178-179℃. ^{1}H NMR (600 MHz, Chloroform-d) δ 7.74 (s, 4 H, pyridyl-H), 7.68 (d, J=4.1 Hz, 4 H, pyridyl-H), 7.65 – 7.37 (m, 2 H, Ar-H), 7.37 – 7.28 (m, 2 H,vinyl-H), 7.14 (ddd, J=17.8, 11.7,4.1Hz, 6 H, Ar-H), 7.09 – 6.94 (m, 2 H, vinyl-H). ^{13}C NMR (100 MHz, Chloroform-d) δ 153.9, 152.7, 150.1, 144.7, 132.3, 131.7, 129.0, 128.7, 128.4, 121.2, 114.3. HRMS (ESI-TOF) m/z: $[M+H]^+$ Calcd for $C_{30}H_{21}N_2$ 409.1616; Found 409.1690.

DPPD-9C: A mixture of compound **DPPD** (0.41 g, 1 mmol) and 1-bromodenonane (10 mmol) was added into DMF (30 mL) and 180℃ (heating mantle) refluxed for 12h. After cooling to room temperature, the precipitant was filtered and washed with DMF and dichloromethane twice time to obtain **DPPD-9C** as a red solid (0.43 g, 52.4%). mp 333-334℃. ^{1}H NMR (600 MHz, DMSO-d6) δ 9.16 (d, J = 18.0 Hz, 2H), 9.07 (d, J = 18.0 Hz, 2H), 9.07 (d, J = 12 Hz, 4H), 8.72 (d, J = 8.3 Hz, 2H), 8.57 (d, J = 6.7 Hz, 4H), 8.52 (d, J = 8.3 Hz, 2H), 8.45 (d, J = 9.3 Hz, 2H), 7.91 (d, J = 15.9 Hz, 2H), 4.56 (t, J = 7.4 Hz, 4H), 2.06-1.89 (m, 4H), 1.43-1.19 (m, 24H), 0.86 (dt, J = 13.8, 6.9 Hz, 6H). HRMS (ESI-TOF) m/z: $[M]^{2+}$ Calcd for $C_{48}H_{58}N_2^{2+}$ 331.2295; found 331.2281.

Both compounds **DPPD-10C** and **DPPD-12C** were synthesized following the same experiment conditions as for **DPPD-9C**.

DPPD-10C: The compound **DPPD-10C** was obtained as a red solid (0.47 g, 55.3%). mp 336-337℃. ^{1}H NMR (600 MHz, DMSO-d6) δ 9.16 (d, J = 15.9 Hz, 2H), 9.06 (m, 6H), 8.72 (d, J = 8.3 Hz, 2H), 8.57 (d, J = 6.6 Hz, 4H), 8.52 (d, J = 8.4 Hz, 2H), 8.45 (d, J = 9.3 Hz, 2H), 7.91 (d, J = 15.9 Hz, 2H), 4.56 (t, J = 7.4 Hz, 4H), 2.09-1.79 (m, 4H), 1.47-1.12 (m, 28H), 0.94-0.74 (m, 6H). HRMS (ESI-TOF) m/z: $[M]^{2+}$ Calcd for $C_{50}H_{62}N_2^{2+}$ 345.2451; found 345.2449.

DPPD-12C: The compound **DPPD-12C** was obtained as a red solid (0.52 g, 58.1%). mp 338-339℃. ^{1}H NMR (600 MHz, DMSO-d6) δ: 9.16 (d, J = 15.9 Hz, 2H), 9.06 (t, J = 8.1 Hz, 6H), 8.72 (d, J = 8.4 Hz, 2H), 8.57 (d, J = 6.7 Hz, 4H), 8.52 (d, J = 8.4 Hz, 2H), 8.45 (d, J = 9.4 Hz, 2H), 7.91 (d, J = 15.8 Hz, 2H),

4.55 (t, J = 7.4 Hz, 4H), 1.96 (m, 4H), 1.29 (m, 36H), 0.84 (t, J = 6.9 Hz, 6H). HRMS (ESI-TOF) m/z: $[M]^{2+}$ Calcd for $C_{54}H_{70}N_2^{2+}$ 373.2764; found 373.2756.

X-ray Crystallography: Crystallographic data for **DPPD** were collected on a Bruker APEX 2 CCD diffractometer with graphite-monochromated Mo Kα radiation (λ = 0.71073 Å) in the ωscan mode.[45] The structures were solved by a charge flipping algorithm and refined by full-matrix least-squares methods on F2.[47,48]. Data for the structures reported here have been deposited with the Cambridge Crystallographic Data Centre with deposition numbers CCDC 2250518, which contain the supplementary crystallographic data for this paper. These data can be obtained free of charge from The Cambridge Crystallographic Data Centre via www.ccdc.cam.ac.uk/data_request/cif.

Supplementary data

Electronic Supplementary Information (ESI) available: Details of the ^{1}H NMR and MS spectra.

AUTHOR INFORMATION

Corresponding Authors

Qi-Long Zhang - *School of Biology and Engineering, Guizhou Medical University, School of Basic Medical Science, Guizhou Medical University , Guiyang 550014, China*; orcid.org/ 0000-0002-5499-267X; Email: gzuqlzhang@126.com

Hong Xu - *School of Biology and Engineering, Guizhou Medical University, School of Basic Medical Science, Guizhou Medical University , Guiyang 550014, China*; orcid.org/ 0009-0006-1173-7421; Email: xuhong@gmc.edu.cn

Xing Feng - *School of Materials and Energy, Guangdong University of Technology, Guangzhou 510006, China*; orcid.org/ 0000-0002-4273-979X; Email: hyxhn@sina.com

Authors

Xu Zhou - *School of Biology and Engineering, Guizhou Medical University, School of Basic Medical Science, Guizhou Medical University , Guiyang 550014, China*
Xiaohui Wang - *School of Materials and Energy, Guangdong University of Technology , Guangzhou 510006, China*
Tian-Yu Zhang - *School of Biology and Engineering, Guizhou Medical University, School of Basic Medical Science, Guizhou Medical University , Guiyang 550014, China*
Lingyi Shen - *School of Biology and Engineering, Guizhou Medical University, School of Basic Medical Science, Guizhou Medical University , Guiyang 550014, China*
Xian-Jiong Yang - *School of Biology and Engineering, Guizhou Medical University, School of Basic Medical Science, Guizhou Medical University , Guiyang 550014, China*
Carl Redshaw - *Chemistry, School of Natural Sciences, University of Hull, Cottingham Road, Hull, Yorkshire HU6 7RX, UK*

Notes

The authors declare no competing financial interest.

Acknowledgements

This word was supported by the National Natural Science Foundation of China (22065009, 22066007, 21975054), the Guizhou Provincial Natural Science Foundation (grant number ZK[2022]395), the Guizhou Province College Students Innovation and Entrepreneurship Project(S202010660036, S202010660014). CR thanks the University of Hull for support.

References

[1] H. G. Nie, Z. Wei, X. L. Ni, Y. Liu, Assembly and Applications of Macrocyclic-Confinement-Derived Supramolecular Organic Luminescent Emissions from Cucurbiturils, Chem. Rev. 2022, **122**, 9032-9077. DOI: 10.1021/acs.chemrev.1c01050.

[2] Y. Lei, Q. Chen, P. R. Liu, L. X. Wang, H. Y. Wang, B. D. Li, X. Y. Lu, Z. Chen, Y. J. Pan, F. H. Huang, H. Li, Molecular Cages Self-Assembled by Imine Condensation in Water, Angew. Chem. Int. Ed. 2021, 60, 4705-4711. DOI: 10.1002/anie.202013045.

[3] M. Bhol, B. Shankar, M. Sathiyendiran, Calix[4]arene-Analogous Technetium Supramolecules, Inorg. Chem. 2022, 61, 11497-11508. DOI: 10.1021/acs.inorgchem.1c03691.

[4] H. X. Zhou, X. D. Pang, Electrostatic Interactions in Protein Structure, Folding, Binding, and Condensation, Chem. Rev. 2018, 118, 1691-1741. DOI: 10.1021/acs.chemrev.7b00305.

[5] S. L. Beshahwured, T. H. Mengesha, L. M. Babulal, Y. S. Wu, S. H. Wu, J. K. Chang, R. Jose, C. C. Yang, Hierarchical Interconnected Hybrid Solid Electrolyte Membrane for All-Solid-State Lithium-Metal Batteries Based on High-Voltage NCM811 Cathodes, ACS Appl. Energy Mater. 2022, 5, 2580-2595. DOI: 10.1021/acsaem.2c00046.

[6] S. H. Wang, Y. Y. Lin, C. Y. Teng, Y. M. Chen, P. L. Kuo, Y. L. Lee, C. T. Hsieh, H. Teng, Immobilization of Anions on Polymer Matrices for Gel Electrolytes with High Conductivity and Stability in Lithium Ion Batteries, ACS Appl. Mater. Interfaces. 2016, 8, 14776-14787. DOI: 10.1021/acsami.6b01753.

[7] T. Liu, Y. Y. Guo, J. H. Wang, J. Wang, L. S. Zhu, J. Zhang, C. Zhang, Assessing toxic effects of [Omim]Cl and [Omim]BF_4 in zebrafish adults using a biomarker approach, Environ. Sci. Pollut. Res. 2016, 23, 7360-7368. DOI: 10.1007/s11356-

015-5887-3.

[8] M. A. Greer, G. Goodman, R. C. Pleus, S. E. Greer, Health effects assessment for environmental perchlorate contamination: the dose response for inhibition of thyroidal radioiodine uptake in humans, Environ. Health Perspect. 2002, 110, 927-937. DOI: 10.1289/ehp.02110927.

[9] H. M. Wang, X. L. Zhang, S. J. Wang, H. Y. Ma, Y. L. Shen, X. Wang, A Multifunctional Electrochemical Sensor for the Simultaneous Detection of Ascorbic Acid, Dopamine, Uric Acid, and Nitrite, J. AOAC Int. 2021, 104, 860-866. DOI: 10.1093/jaoacint/qsaa157.

[10] Mounesh, K. R. V. Reddy, Sensitive and reliable electrochemical detection of nitrite and H_2O_2 embellish-CoPc coupled with appliance of composite MWCNTs, Anal. Chim. Acta. 2020, 29, 98-107. DOI: 10.1016/j.aca.2020.02.057.

[11] L. J. Jiang, Y. Bao, L. Guo, H. Cui, Q. Wang, K. Liu, X.X. Hao, R. C. Qiu, Z. Y. Guo, Y. Fa, Simultaneous Detection of Anions and Carbohydrates in Cyanobacteria by Two-Dimensional Ion Chromatography, J. AOAC Int. 2021, 104, 1408-1414. DOI: 10.1093/jaoacint/qsaa153.

[12] N. Nakatani, D. Kozaki, M. Mori, K. Tanaka, Recent progress and applications of ion-exclusion/ion-exchange chromatography for simultaneous determination of inorganic anions and cations, Anal. Sci. 2012, 28, 845-852. DOI: 10.2116/analsci.28.845.

[13] A. Mondal, S. Nag, P. Banerjee, Coumarin functionalized molecular scaffolds for the effectual detection of hazardous fluoride and cyanide, Dalton Trans. 2021, 50,

429-451. DOI: 10.1039/d0dt03451g.

[14] Z. J. Xu, W. X. Shi, C. J. Yang, J. Xu, H. P. Liu, J. Xu, B. C. Zhu, A colorimetric AIEgens for rapid and specific detection of nitrite, Luminescence. 2020, 35, 299-304. DOI: 10.1002/bio.3727.

[15] D. Wu, A. C. Sedgwick, T. Gunnlaugsson, E. U. Akkaya, J. Y. Yoon, T. D. James, Fluorescent chemosensors: the past, present and future, Chem. Soc. Rev. 2017, 46, 7105-7123. DOI: 10.1039/c7cs00240h.

[16] A. A. Rajapaksha, Y. X. Fu, W. Y. Z. Guo, S. Y. Liu, Z. W. Li, C. Q. Xiong, W. C. Yang, G. F. Yang, Review on the recent progress in the development of fluorescent probes targeting enzymes, Methods Appl. Fluoresc. 2021, 9, 032001. DOI: 10.1088/2050-6120/abf988.

[17] Y. N. Liu, X. H. Feng, Y. A. Yu, Q. Y. Zhao, C. H. Tang, J. M. Zhang, A review of bioselenol-specific fluorescent probes: Synthesis, properties, and imaging applications, Anal. Chim. Acta. 2020. 1110, 141-150. DOI: 10.1016/j.aca.2020.03.027.

[18] S. Chowdhury, B. Rooj, A. Dutta, U. Mandal, Review on Recent Advances in Metal Ions Sensing Using Different Fluorescent Probes, J. Fluoresc. 2018, 28, 999-1021. DOI: 10.1007/s10895-018-2263-y.

[19] M. Ehsan, R. Rahmatollah, S. Vahid, Sonochemically synthesized microporous metal-organic framework representing unique selectivity for detection of Fe^{3+} ions, Polyhedron. 2019, 159, 251-258. DOI: 10.1016/j.poly.2018.11.062.

[20] K. Sima, S. Vahid, Carbon dioxide capture in MOFs: The effect of ligand

functionalization, Polyhedron. 2018, 154, 236-251. DOI: 10.1016/j.poly.2018.07.042.

[21] J. W. Steed, Anion-tuned supramolecular gels: a natural evolution from urea supramolecular chemistry, Chem. Soc. Rev. 2010, 39, 3686-3699. DOI: 10.1039/b926219a.

[22] D. X. Wang, M. X. Wang, Exploring Anion-π Interactions and Their Applications in Supramolecular Chemistry, Acc. Chem. Res. 2020, 53, 1364-1380. DOI: 10.1021/acs.accounts.0c00243.

[23] J. T. Davis, P. A. Gale, R. Quesada, Advances in anion transport and supramolecular medicinal chemistry, Chem. Soc. Rev. 2020, 49, 6056-6086. DOI: 10.1039/c9cs00662a.

[24] S. Mandal, A. Sahana, A. Banerjee, D. A. Safin, M. G. Babashkina, K. Robeyns, S. Verkaart, J. G. J. Hoenderop, M. P. Mitoraj, Y. Garcia, D. Das, A smart rhodamine-pyridine conjugate for bioimaging of thiocyanate in living cells, RSC Adv. 2015, 5, 103350-103357. DOI: 10.1039/C5RA21838A.

[25] S. Nandi, A. Sahana, S. Mandal, A. Sengupta, A. Chatterjee, D. A. Safin, M. G. Babashkina, N. A. Tumanov, Y. Filinchuk, D. Das, Hydrazine selective dual signaling chemodosimetric probe in physiological conditions and its application in live cells, Anal. Chim. Acta. 2015, 893, 84-90. DOI: 10.1016/j.aca.2015.08.041.

[26] J. D. Luo, Z. L. Xie, J. W. Y. Lam, L. Cheng, H. Y. Chen, C. F. Qiu, H. S. Kwok, X. W. Zhan, Y. Q. Liu, D. B. Zhu, B. Z. Tang, Aggregation-induced emission of 1-methyl-1,2,3,4,5-pentaphenylsilole, Chem. Commun. 2001, 18, 1740-1741. DOI:

10.1039/b105159h.

[27] J. Mei, Y. H. Huang, H. Tian, Progress and Trends in AIE-Based Bioprobes: A Brief Overview, ACS Appl. Mater. Interfaces. 2018 , 10, 12217-12261. DOI: 10.1021/acsami.7b14343.

[28] R. Y. Zhan, Y. T. Pan, P. N. Manghnani, B. Liu, AIE Polymers: Synthesis, Properties, and Biological Applications, Macromol. Biosci. 2017, 17, 1600433. DOI: 10.1002/mabi.201600433.

[29] D. Wang, M. M. S. Lee, G. G. Shan, R. T. K. Kwok, J. W. Y. Lam, H. F. Su, Y. C. Cai, B. Z. Tang, Highly Efficient Photosensitizers with Far-Red/Near-Infrared Aggregation-Induced Emission for In Vitro and In Vivo Cancer Theranostics, Adv Mater. 2018, 30, e1802105. DOI: 10.1002/adma.201802105.

[30] Y. Y. Yuan, G. X. Feng, W. Qin, B. Z. Tang, B. Liu, Targeted and image-guided photodynamic cancer therapy based on organic nanoparticles with aggregation-induced emission characteristics, Chem. Commun. 2014, 50, 8757-8760. DOI: 10.1039/c4cc02767a.

[31] S. M. Lee, C. H. Chen, A. H. Flood, A pentagonal cyanostar macrocycle with cyanostilbene CH donors binds anions and forms dialkylphosphate[3]rotaxanes, Nat. Chem. 2013, 5, 704-710. DOI: 10.1038/nchem.1668.

[32] R. Kumar, S. Kumar, P. Singh, G. Hundal, M. S. Hundal, S. Kumar, A fluorescent chemosensor for detection of perchlorate ions in water, Analyst, 2012, 137, 4913-4916. DOI: 10.1039/c2an35901d.

[33] P. Singh, L. S. Mittal, V. Vanita, R. Kumar, G. Bhargava, A. Walia, S. Kumar, Bay

functionalized perylenediimide as a deaggregation based intracellular fluorescent probe for perchlorate, Chem. Commun. 2014, 50, 13994-13997. DOI: 10.1039/c4cc06765g.

[34] S. Y. Chen, X. L. Ni, Development of an AIE based fluorescent probe for the detection of nitrate anions in aqueous solution over a wide pH range, RSC Adv. 2016, 6, 6997-7001. DOI: 10.1039/C5RA23369K.

[35] Y. P. Yang, S. Y. Chen, X. L. Ni, Anion Recognition Triggered Nanoribbon-Like Self-Assembly: A Fluorescent Chemosensor for Nitrate in Acidic Aqueous Solution and Living Cells, Anal. Chem. 2015, 87, 7461-7466. DOI: 10.1021/acs.analchem.5b01774.

[36] X. Gong, Q. L. Zhang, S. Zhang, Y. Xi, Q. H. Bai, S. Y. Chen, X.L. Ni, A cationic fluorescent probe for BF_4^- and PF_6^- anions by aggregation self-assembly: An efficient approach to recognition of anions in aqueous solution, Dyes Pigm. 2019, 163, 5 02-508. DOI: 10.1016/j.dyepig.2018.12.038.

[37] S. Y. Su, Z. Q. Zheng, Q. L. Zhang, X. L. Ni, Fatty-chain-switched cationic fluorescent probe for SCN^- , PF_6^-, and HSO_3^- recognition in water: Study of anion selectivity and sensitivity, Dyes Pigm. 2021, 185, 108903. DOI: 10.1016/j.dyepig.2020.108903.

[38] X. Zhang, S. Y. Su, X. T. Chen, L. Y. Shen, Q. L. Zhang, X. L. Ni, H. Xu, Z. Y. Wang, C. Redshaw, A New Cationic Fluorescent Probe for HSO_3^- Based on Bisulfite Induced Aggregation Self-Assembly, Molecules. 2022, 27, 2378. DOI: 10.3390/molecules27082378.

[39] M. M. Islam, Z. Hu, Q. S. Wang, C. Redshaw, X. Feng, Pyrene-based Aggregation-induced Emission Luminogens and their Applications, Mater. Chem. Front. 2019, 3, 762-781. DOI: 10.1039/C9QM00090A.

[40] X. Feng, J. Y. Hu, C. Redshaw, T. Yamato, Functionalization of Pyrene to Prepare Luminescent Materials-Typical Examples of Synthetic Methodology, Chem. - Eur. J. 2016, 22, 11898-11916. DOI: 10.1002/chin.201643197.

[41] X. H. Wang, J. Y. Zhang, X. Y. Mao, Y. W. Liu, R. K. Li, J. Bai, J. Zhang, C. Redshaw, X. Feng, B. Z. Tang, Intermolecular Hydrogen-Bond-Assisted Solid-State Dual-Emission Molecules with Mechanical Force-Induced Enhanced Emission, J. Org. Chem. 2022, 87, 8503-8514. DOI: 10.1021/acs.joc.2c00617.

[42] X. Y. Mao, F. L. Xie, X. H. Wang, Q. S. Wang, Z. P. Qiu, M. R. J. Elsegood, J. Bai, X. Feng , C. Redshaw, Y. P. Huo, J. Y. Hu, Q. Chen, New Quinoxaline-Based Blue Emitters: Molecular Structures, AggregationInduced Enhanced Emission Characteristics and OLED Application, Chin. J. Chem. 2021, 39, 2154-2162. DOI: 10.1002/cjoc.202100157.μm

[43] K. J. Rothschild, I. M. Asher, H. E. Stanley, E. Anastassaki, Raman spectroscopy of uncomplexed valinomycin. 2. Nonpolar and polar solution, J. Am. Chem. Soc. 1977, 99, 2032-2039. DOI: 10.1021/ja00449a003.

[44] X. H. Wang, C. J. Zhang, J. Zeng, X. Y. Mao, C. Redshaw, G. L. Niu, X. Q. Yu, X. Feng, One-Pot Synthesis of Pyreno[2,1-b]furan Molecules with Two-Photon Absorption Properties, J. Org. Chem. 2022, 87, 12741-12748. DOI: 10.1021/acs.joc.2c01303.

[45] J. G. Wang, X. G. Gu, P. F. Zhang, X. B. Huang, X. Y. Zheng, M. Chen, H. T. Feng, R. T. K. Kwok, J. W. Y. Lam, B. Z. Tang, Ionization and Anion-π^+ Interaction: A New Strategy for Structural Design of Aggregation-Induced Emission Luminogens, J. Am. Chem. Soc. 2017, 139, 16974-16979. DOI: 10.1021/jacs.7b10150.

[46] 36SAINT and APEX 2 software for CCD diffractometers. Bruker AXS Inc., Madison, USA, 2015.

[47] G. M. Sheldrick, SHELXT - Integrated space-group and crystal-structure determination, Acta Cryst., 2015, A71, 3–8. DOI: 10.1107/S2053273314026370.

[48] A. L. Spek, PLATON SQUEEZE: a tool for the calculation of the disordered solvent contribution to the calculated structure factors, Acta Cryst.,2015, C71, 9–18. DOI: 10.1107/S2053229614024929.

Graphical abstract